Physica E 136 (2022) 115037

Contents lists available at ScienceDirect

Physica E: Low-dimensional Systems and Nanostructures

journal homepage: www.elsevier.com/locate/physe

DFT studies on PbO_2 and binary PbO_2/SnO_2 thin films

G.S.L. Fabris [a], D.H.M. Azevedo [b], A.C. Alves [b], C.A. Paskocimas [a], J.R. Sambrano [c], J.M. M. Cordeiro [b,*]

[a] Department of Materials Engineering, Federal University of Rio Grande do Norte, 59078-970, Natal, RN, Brazil
[b] Department of Physics and Chemistry, School of Natural Sciences and Engineering, São Paulo State Universtiy (UNESP), 15385-000, Ilha Solteira, Brazil
[c] Modeling and Molecular Simulation Group, São Paulo State University, 17033-360, Bauru, SP, Brazil

ARTICLE INFO

Keywords:
PbO_2
SnO_2
Binary films
DFT
Semiconductors
Surface stability

ABSTRACT

Periodic quantum mechanics DFT calculations have been employed to investigate surface and electronic properties of β-PbO_2 thin films and binary β-PbO_2/SnO_2 thin films with crystallographic planes (001), (010), (101), and (110) in both cases. The results show significant increases in the band gap energy of the pure PbO_2 films compared to that of the bulk, due to a marked increase in the minimum energy of the conduction band. The relative surface stability follows the sequence (110) > (101) > (010) > (001). The surfaces become more unstable, and with a more accentuated ionic character after coating with SnO_2, however, the relative stability of the surfaces does not change. Thus, the preferential growth direction and the crystalline shape of the coated films are maintained. The SnO_2 coating causes significant changes in the band gap, with increases in the films with (001) and (010) surfaces, while a decrease is noticed in the band gap energy of the films with (110) and (101) surfaces.

1. Introduction

Semiconductor metal oxides thin films have been the subject of too much investigation in the last decade, thanks to the possibility of applications in advanced fields such as optoelectronic, catalysis, sensing and solar cells [1–8]. The films can be built of a single oxide or be mounted by layers of different oxides and grown according to distinct geometries and crystallographic directions. In the case of combination of different materials, the superposition can affect the electronic structure and the surface properties of each one, resulting in a high-performance composite for a specific application [9–12]. Of course, the properties of the system will depend on the individual materials used for mount the film and can be remarkable unique consonant to the individual properties of the components. Some of these systems have been the subject of a series of experimental and theoretical studies performed in our group, as it has been reported in the last few years [6–8,13], and new ones continue to be looked for. In the present work, the scrutiny is upon the PbO_2/SnO_2 rutile system. Although these oxides share a common crystalline structure (rutile), which facilitates the mounting, they have tremendously different electric properties.

Rutile β-PbO_2 (plattnerite) can be prepared in different phase structures and doped in different ways [14]. It is intrinsically metallic or a narrow band gap semiconductor [15–17], with a band gap energy of 0.61eV and a carrier concentration in the order of 10^{20} - 10^{21} cm^{-1} [18]. Typically displays degenerate n-type conductivity assigned to oxygen vacancies [17,19], and although opaque (thanks to its low band gap) it can potentially become a transparent conducting oxide (TCO) [20–22], as it has already been observed with other materials.[23-25] This result is achieved with the blue-shift of the optical band gap, according to the Moss-Burstein effect.[26,27] The optical transparency is guaranteed since the transitions from the bottom filled conduction band states to the next highest conduction band lie above the threshold for visible light absorption.[23,28,29] Thin films of β-PbO_2 have received special attention mainly because of its chemical stability and the possibility of preparing in a wide range of surface morphologies [30,31]. Electrodes of β-PbO_2 have been used for electrochemical degradation of organic pollutants and production of ozone [32,33]. Controversies on the realm PbO_2 electronic character have arised in recent years due to its tiny band gap energy [34–36]. Accordingly to these discussions β-PbO_2 is being considered a topological material behaving as a 3D Dirac semimetal if spin-orbit coupling is considered. Thus, β-PbO_2 seems to provide a good environment for exploring physical properties of Dirac semimetals, which can be an auspicious field of study in the near future.

On the other hand, SnO_2 thin films are transparent and thermally stable and have been too much studied some years ago due to the possibilities for applications as fore-contacts in superstrate heterojunction

* Corresponding author.
E-mail address: joao.cordeiro@unesp.br (J.M.M. Cordeiro).

https://doi.org/10.1016/j.physe.2021.115037
Received 13 September 2021; Accepted 27 October 2021
Available online 28 October 2021

solar cells, opto-electronic devices technology, photocatalysis and gas sensors, applications in which a high transmittivity in the visible-infrared range is required [37–40]. Undoped SnO_2 is an n-type semiconductor with a band gap energy of about 3.6 eV at room temperature [41,42]. The electrical conductivity depends on deviation from stoichiometry, leading to oxygen vacancies, interstitial tin atoms, and oxygen adsorption at surface and grain boundary [43,44]. The conductivity can also be modulated by doping. For instance, doping SnO_2 with pentavalent ions as Sb^{5+} leads to increased conductivity due to the substitution of Sn^{4+} in the SnO_2 matrix [45,46]. Optical and electronic properties of SnO_2 have been subject of persistent examination both theoretical and experimentally [47–53]. In spite of that, as well as with β-PbO_2, its band structure and other related optical properties are still upon debate [54–59].

Computational modeling and simulation have proved to be useful tools to assist experimentalists to understand their results and develop new materials with specific or poorly studied properties. Some of these techniques have been used in our group to study the most diverse systems [60–63]. In a recent study, theoretical investigations of surface and electronic structures of TiO_2 films coated with PbO_2 have been performed through density functional theory (DFT) calculations [13], using the B3LYP hybrid density functional [64,65] with Grimme approaching [66,67] to describe the long-range weak interactions. At work now, the study is being extended to PbO_2 thin films coated with SnO_2 (PbO_2/SnO_2), both in the tetragonal rutile phase. As far as we know, this is the first time this system is being investigated. Bulk of both neat PbO_2 and SnO_2 and surfaces of neat PbO_2 have also been simulated for comparison. The films were grown in the crystallographic directions [110], [101], [010], and [001], and the analysis done in terms of optimized geometric parameters, band structure, density of states (DOS), distribution of charge density, and surfaces order stability of the nude and coated films.

2. Model system and computational procedure

Both oxides have a crystalline rutile structure that belongs to the tetragonal space group ($P4_2/mnm$), with cell parameters a and c, and internal u parameter, which is the vertical distance between oxygen and the metal atom, as shown in the Fig. 1. The experimental cell parameters of PbO_2 are $a = c = 4.958$ Å, $b = 3.338$ Å, and $u = 0.296$ Å [18], while for SnO_2 those values are $a = c = 4.737$ Å, $b = 3.185$ Å, and $u = 0{,}307$ Å [68].

According to the procedure described previously [23], both bulk structures were optimized by the use of analytical energy gradients with respect to both atomic coordinates and unit cell parameters. The simulations were performed using the periodic DFT implemented in the CRYSTAL17 program [69], which use crystalline orbitals represented as a linear combination of Bloch functions defined in terms of Gaussian-type basis set local functions (atomic orbitals) [70]. A full optimization procedure (parameters a, b, and c, and inner coordinate u) was carried out to determine the equilibrium geometry. In order to achieve the best modeling, a couple of different basis sets which are available in the CRYSTAL webpage (https://www.crystal.unito.it/basis-sets.php) were tested both for Pb and Sn (see Table 1 and ref. 13). Both metals were treated in the framework of core pseudopotential approximation, because the number of electrons makes the simulations very expensive. The basis set used for oxygen was 6-31d1 for both the oxides [71].

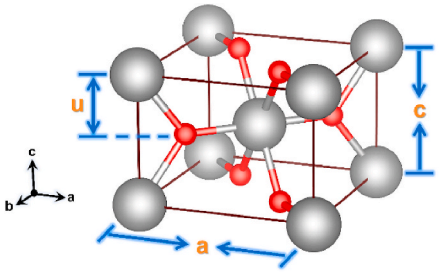

Fig. 1. The conventional rutile unit cell (grey: Pb or Sn; red: O).

DFT is a methodology with a great capacity of depicting the structural, energetic and electronic properties of solid states materials with high accuracy in combination with hybrid functionals based on the generalized gradient approximation (GGA) [72,73]. Even though there are several functionals available to perform these kind of calculations, it is difficult to find one that describe accurately electronic and structural properties at the same time [74–77]. Thus, the choice of a proper functional is basilar to the realistic simulation of the properties of the materials. B3LYP [64,65], one of the most popular functionals used for studying solids among the hybrid functionals available, has been chosen to the present calculations. A deep analysis on the reproducibility of DFT calculations of solids has been published in recent years [78,79].

The minimized structures were characterized by diagonalizing the Hessian matrix with concerning to the lattice parameters and atomic coordinates; and the convergence of the nuclear displacements and gradient components were checked with tolerances on their root-mean-squares set to 0.001 and 0.004 a.u., respectively. The level of accuracy of the Coulomb and the exchange series calculation is controlled by five parameters, α_i, with $i = 1$–5, such that two-electron contributions are neglected when the overlap between atomic functions is below $10^{-\alpha_i}$, in which the threshold 10, 10, 10, 10 and 20 were chosen for the Coulomb overlap, Coulomb penetration, exchange overlap, first exchange pseudo-overlap, and second exchange pseudo-overlap, respectively. The shrinking (Monkhorst-Pack and Gilat) [80] factor was set up to 10. To model the experimental thin films, slabs were "built" from the bulk with the geometry previously optimized. The bulk was cut in the crystallographic directions [110], [101], [010], and [001], making a two-dimensional structure with a finite number of layers (thickness) in the chosen direction. The number of layers has been defined accordingly to study performed previously [13,72]. The values of the slabs thickness after relaxation are reported in Table 3. So, the thickness must be such that the properties of the central region of the slab converge to those of the bulk. Further details upon the slabs modeling can be found in a previous report [13]. The slabs are then submitted to geometry optimization with respect to the atomic coordinates only to allow relaxation of the surface atoms and minimize the energy.

Once the pure PbO_2 slabs have been optimized, Pb atoms were substituted for Sn atoms on the two first layers of both the surfaces and the optimization procedure was repeated. A scheme of the simulated pure slabs and the surface Pb/Sn substituted ones is represented in Fig. 2.

Having the minimized slabs on hands, one can calculate the surface energy (E_{surf}). Surface energy ($J.m^{-2}$) can be defined as the surface excess free energy per unit area and is an important indicator of surface stability and reactivity in addition to inform on crystal equilibrium shapes [81]. The surface energy E_{surf} ($J.m^{-2}$) is defined as the difference between the slab and the bulk energies, divided by the surface area, that is, $E_{surf} = (E_{slab} - E_{bulk})/2A$, were E_{slab} and E_{bulk} are the total slab and bulk energies, respectively, bulk and slabs with the same number of atoms and stoichiometry, and A is the surface area of one side of the slab [82] (the factor 2 is due to the film having two faces). In the case of coated films, a small change has to be done in the equation used to calculate the surface energy, which becomes: $E_{surf} = (E_{slab} - n_1 E_{PbO_2} - n_2 E_{SnO_2})/2A$, where E_{PbO_2} and E_{SnO_2} are the energies of the PbO_2 and SnO_2 bulks, and n_1 and n_2 are the numbers of PbO_2 and SnO_2 units in the slab, respectively.

Using the crystalline lattice parameters and the theoretical surface energies obtained (E_{surf}), it is possible to study the morphology of the PbO_2 and PbO_2/SnO_2 crystals using the classical Wulff's construction theory [83]. The Wullf construction is based on the assumption that a

Table 1
Experimental and calculated structural parameters (Å), and band gap energy (eV) for bulk rutile SnO_2 using different basis sets for Sn, and the respective deviation (%) to experimental value.

Basis set	a	Δa	c	Δc	u	Δu	E_{gap}	ΔE_{gap}
DB-21G*[89]	4.6849	−1.10	3.1578	−0.86	0.3059	−0.36	3.8084	5.75
DB-21G [90]	4.6720	−1.37	3.1622	−0.72	0.3060	−0.34	3.8222	6.17
POB_DZVP [91]	4.7146	−0.47	3.2213	1.14	0.3061	−0.31	4.5457	26.27
Experimental [68]	4.7370	–	3.1850	–	0.3070	–	3.6	–

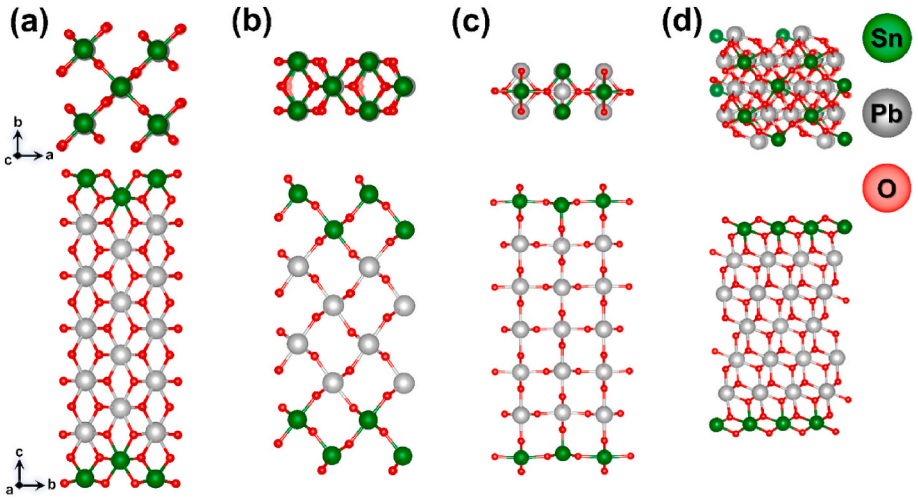

Fig. 2. Schemes of the (a) (0 0 1), (b) (0 1 0), (c) (1 1 0) and (d) (1 0 1) surface films. In the pure PbO_2 films all metallic atoms are Pb.

crystal grows minimizing the Gibbs free energy of its surfaces. As the surface energy of a plane is proportional to its distance from the center of the crystal, the growth of the crystal in a direction is inversely proportional to the surface energy perpendicular to that direction. Wulff's calculation has been successfully used to obtain the morphology of other materials [84–87].

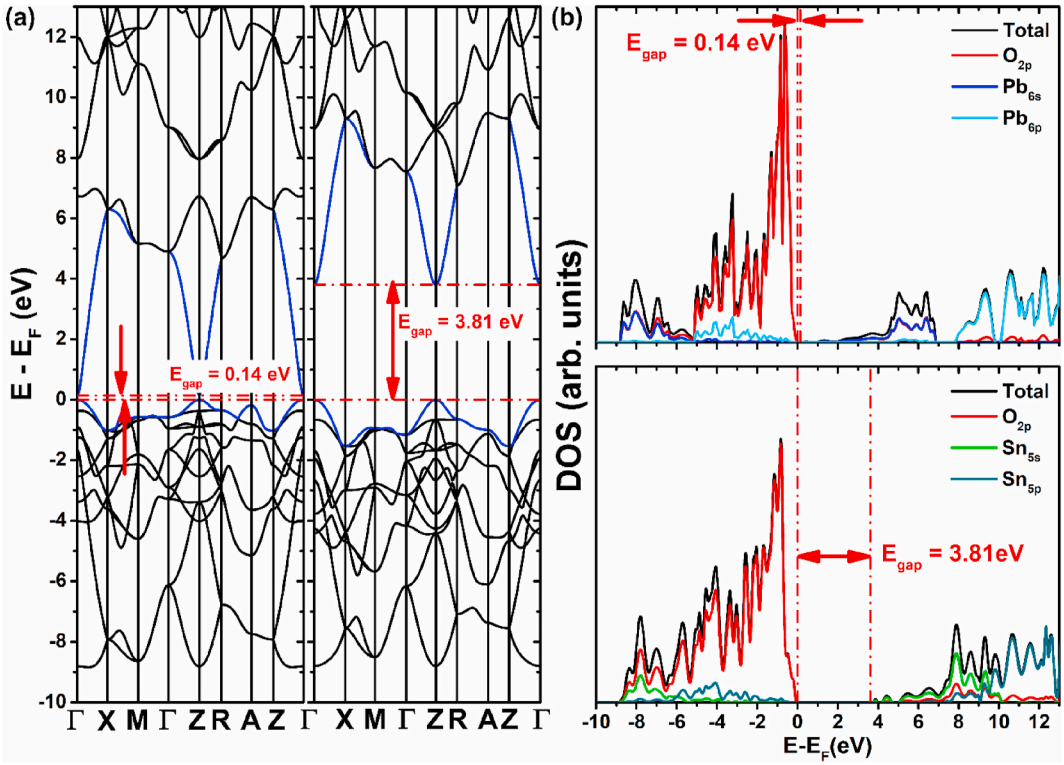

Fig. 3. (a) Band structures of PbO_2 (left) [13] and SnO_2 (right) bulks, and (b) total and partial DOS diagram for PbO_2 (above) and SnO_2 (below).

3. Results and discussion

3.1. Bulk

Table 1 lists the experimental values and the calculated lattice parameters, inner coordinate, and band gap energy obtained for bulk SnO_2 with different basis sets used for Sn. It is observed that the DB-21G* (where DB refers to the Durand-Barthelat's pseudopotential) is a good basis set to fit the experimental results of SnO_2 and was chosen to perform the remaining calculations. According to previously reported results [13] the Pb DB-31G*[88] is the basis set that better reproduce the PbO_2 behaviour, and has been used in the present calculations now.

Once identified the best basis set to model the oxides, one can proceed to explore their properties theoretically. The band structure of the bulk of both materials is shown in Fig. 3 to be used as a reference for later comparison. The band structures were calculated along the high symmetry path of the Brillouin zone. Both oxides present a direct band gap at Γ point, being the band gap energy of 0.14 eV for PbO_2 and 3.80 eV for SnO_2, which is in good agreement with experimental values [18,68]. As it has been pointed out in the introduction, the Γ point conic structure of PbO_2 resembles a Dirac cone [34–36], which motivates a deepening in the study of β-PbO_2 topological properties. Looking at both the band structures, the great similarity between them stands out. In both cases the upper valence bandwidth is about 9 eV, in accordance with theoretical values reported previously [16,18,68]. In addition, both oxides have quite like bottom of the conducting bands, differing in the value of the gap between the bottom of the band to the next lower portion of it on the Γ-point. While in SnO_2 that value is about 5.14 eV in the PbO_2 it is 7 eV. Thus, both oxides have the conducting band structure in the Γ-point required to act as TCO, but SnO_2 is more easily turned into since its value of this gap is closer to the energy of the visible region of the electromagnetic radiation than PbO_2. As it has been discussed previously, the transparency of oxides that has a conduction band with that feature could be manipulated, for instance, controlling the oxygen vacancies or doping, thanks to move the electron chemical potential inside the conduction band, and, consequently, changing the optical band gap energy [20,24,25].

Once the oxide band structure is calculated, it is in our best interest to determine which atomic orbitals give rise to this structure. Thus, it has been calculated the projected density of states (PDOS) profiles of each oxide and detail the contribution of the frontier atomic orbitals to the conducting behaviour of each of them. The profiles are shown in the Fig. 3 and compare well with other previously published results [15,16,92–96].

It is clear that in both cases the top of the valence band is formed by the oxygen 2*p* orbitals, which, because of their strong localization, lead to a small hole effective mass [97], which is also related to the conical shape of the band structure at the gamma point. Regarding to the conduction band, while in PbO_2 it is basically composed of Pb *s* and *p* orbitals, the Sn *p* orbital is much less relevant in the SnO_2 conduction band. Another very significant difference between the DOS of the two oxides is the low energy of the Pb conducting orbitals leading to the tiny PbO_2 band gap and the pronounced gap of about 1 eV in the conduction band (about 7–8 eV), separating the Pb 6*s* and 6*p* orbitals, as it has already been found previously [16]. Also noteworthy is the perfect overlap between the O 2*p* orbits and Pb 6*s* in the 2–7 eV energy range of the conduction band, which is a strong indication of an almost complete hybridization of these orbitals. These striking differences in the conduction bands of the two oxides help to understand the huge difference in electrical conductivity between them.

The natural metallic ions are formally closed shells in both oxides (the outer *s* and *p* orbitals are formally empty). However, the electric conduction is due to electrons distributed through these orbitals, as it is shown in the DOS diagram. Thus, it may be useful to have a look at the charge distributed by these orbitals, as a way of comparing their contribution to conductivity in each case. For this purpose, it was raised the electronic charges on each orbital, through the Mulliken population analysis (MPA). Choosing MPA to perform the partition of the charge density is arbitrary, since there are other methods for doing this. However, when comparing different systems, the particular scheme used is not so relevant, since the defects and virtues of that scheme will affect both systems equally. The basis set used for Pb and Sn atoms have 4 electrons located in a *sp* orbital, in addition to another *sp* and 1 *d* empty orbitals. The charge distribution across the atomic orbitals after the simulations is shown in Table 2. As it can be seen, there are no charge located in *d* orbitals at the end of the simulations, which is in agreement with the absence of *d* orbitals in the shown DOS profiles.

From the data in the table is easily realized that the electronic charge distribution in the Pb explicit orbitals is greater than in the Sn ones. And, not only the frontier orbitals in Pb are more occupied, as, thanks to its high atomic number, those electrons are further away from the nucleus, which could be at the root of the PbO_2 greater conductivity. On the other hand, the atomic charge distribution is Pb = +1.945|e|, O = −0.973|e|, and Sn = +2.322|e|, O = −1.161|e|, for PbO_2 and SnO_2 respectively. The Pb and Sn electronic charges are in line with the electronegativity of each atom (Pb = 2.33; Sn = 1.96). It is seen, therefore, that PbO_2 is more covalent than SnO_2, which also contribute for a greater conductivity of the first.

3.2. PbO_2 surfaces

From now on we will focus the attention on the PbO_2 surfaces, to later investigate the changes that are caused in the films by the SnO_2 coating. In general, oxide films can exhibit properties quite different from those of their bulks, including large variations in the values of the band gap energy compared to those of the bulk, and transitions between direct and indirect type [98,99]. The surface structure of metal oxides has a stronger influence on their properties than other elementary semiconductors, due to the symmetry broken and the mixture of ionic and covalent bonds [100]. Slabs were built from the optimized structure of the bulks, as it has already been mentioned, and the respective calculated band structures are shown in the Fig. 4. The band structure was calculated along the Γ– Γ high symmetry path of the slabs Brillouin zone and can be compared with the left side Γ– Γ interval of the bulk structure (Fig. 3). Since the atoms in the slabs are subjected to a large number of different neighbourhoods, the number of lines in the profile of the band structure is very large compared to the profile of the bulk, which requires reducing the plotted range of energy.

The results show significant increases in the band gap energy of the films compared to that of the bulk, which suggests possible new applications for films, unfeasible for pure bulk. The change of the band gap energy ($E_{g/slab}$-$E_{g/bulk}$) (ΔE_g/eV) is 0.95, 0.79, 0.55, and 0.33 for the (010), (101), (001), and (110) surfaces, respectively. Studies on the effect of doping and vacancies on the behavior of such films are on the horizon. Interestingly, the ΔE_g of the surfaces in relation to the bulk, present the same pattern of dependence on the number of coordination of the Pb atom as verified in previous work for TiO_2, with the same rutile-type structure [13], that is, surfaces with the metal atom 5-fold coordinated ((010) and (101)) have the greater ΔE_g, followed by the 4-fold surfaces ((001)), and finishing with the (110) surface, which is 5- and 6-fold coordinated, that has the lower ΔE_g. This finding suggests that the dependence between the metal coordination number and the slab band gap energy discussed in that report [13] applies to other rutile-type oxides, stepping up our attempt to rationalize the relative

Table 2
Orbital charge distribution (m|e|) for Pb and Sn atoms. 2 shells and 8 atomic orbitals, accordingly to the basis set used for each one.

	s	p_x	p_y	p_z	s	p_x	p_y	p_z
Pb	862	225	225	242	247	114	114	027
Sn	553	247	247	266	269	057	057	−070

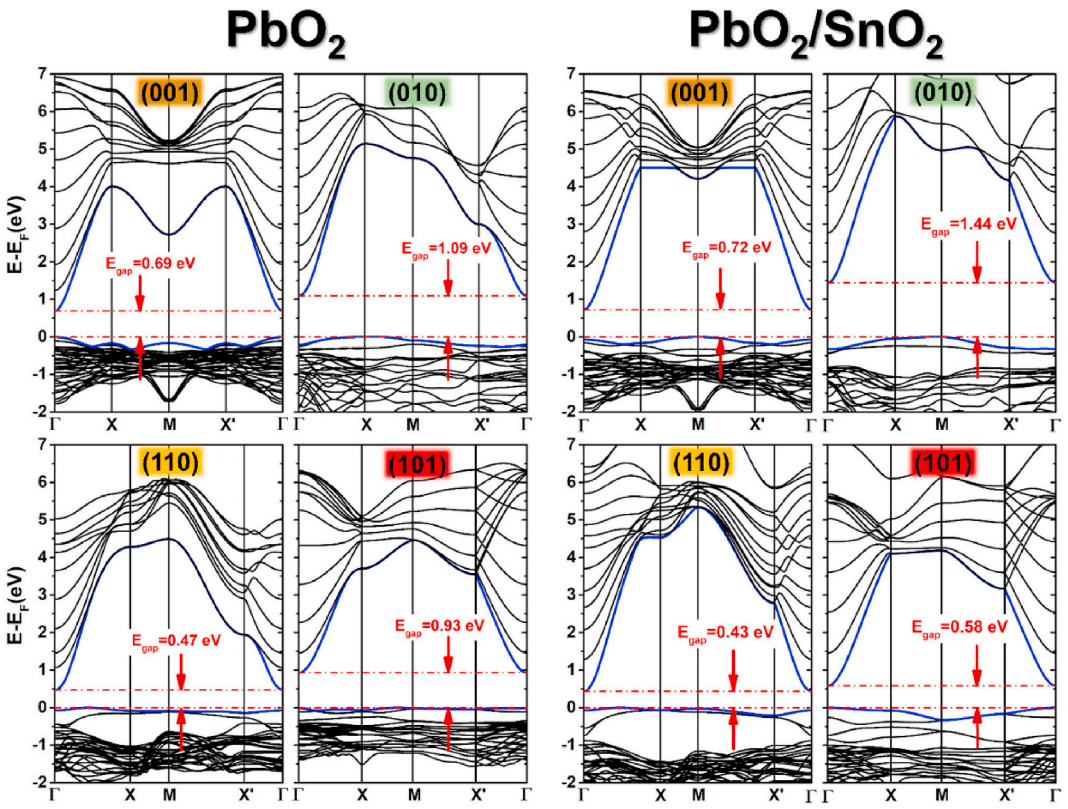

Fig. 4. Band structure of the PbO_2 (left) and PbO_2/SnO_2 (right) surfaces: (0 0 1), (0 1 0), (1 1 0), and (1 0 1).

variation of the oxide film band gap, when compared to the oxide bulk, in terms of the film crystalline direction. A deeper understanding of why this occurs should be sought.

Having that in mind, the DOS profiles of each surface were calculated aiming to detail the contribution of atomic orbitals to the band structure, and the results are shown in the Fig. 5.

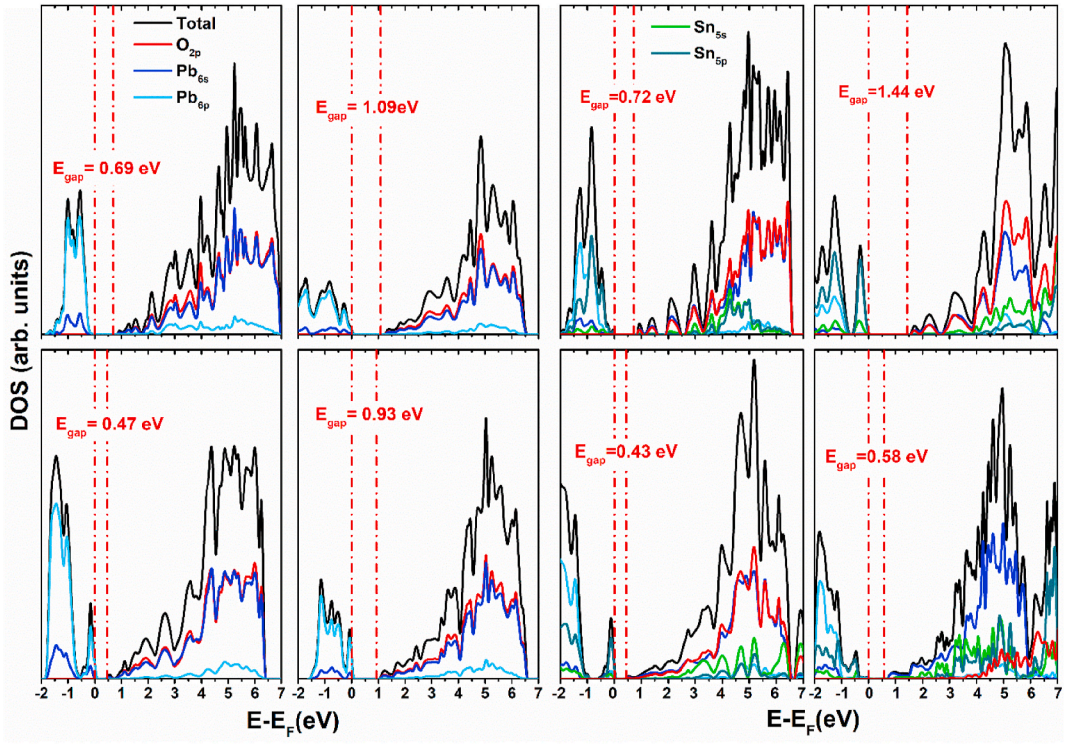

Fig. 5. Total and partial DOS diagram for neat PbO_2 (left) and PbO_2/SnO_2 (right) surfaces (in this case, the O 2*p* and DOS total curve has been supressed in the region of valence band for clarity): (0 0 1), (0 1 0), (1 1 0) and (1 0 1). Y axis is in arbitrary units.

Just like to the bulk, the valence band is mainly constituted of O 2p orbitals, whereas O 2p and Pb 6s are the main contributions for the conduction pattern. The slab structure does not change the relative position of the orbitals compared to the bulk. It is noted that the structure of the valence band is more dependent on the structure of the surfaces. However, there is a marked variation in the minimum energy of the conduction band, which leads to increases in the system band gap, quite significant for some surfaces. This is an important change in the properties of PbO_2 films, compared to the bulk behaviour.

Table 3 lists the MPA on the Pb and O atoms in the firsts four surface layers of the pure PbO_2 slabs. The atomic charges variation depending on the surface and layers is due to the different environments in which the atoms are found in each case.

Firstly, as it would be expected, the Pb and O atomic charges do not cancel each other (the electric neutrality is satisfied in the total film), which implies that each surface has its own polarity and an own excess of positive or negative charge [101,102]. Of course, this will influence the chemical and physical properties of the surface. Secondly, it is noticed a correlation between coordination number and metal atom charge, in the sense that the metal atom has a greater positive electrical charge in the surfaces where it has a higher coordination. On the other hand, the Pb charge for the four layers listed in Table 3 shows a charge migration from the inner of the film to the surface atoms, a reflex of the symmetry broken in the charge distribution. As a consequence, the films are less oxidant and the atom bonds are more covalent than the bulk itself. Of course, the interpretation of the role of the surface characters in the films properties is not trivial, since in the real systems there will always be interaction between the surfaces and the environment.

Clearly, since the distribution of atoms and atomic charges on the surfaces depends on the growth direction of the films, the energy of the surfaces, and, consequently, their stability will vary on the different surfaces. The computed surface energies for the studied surfaces is listed in the Table 4 in the crescent order of energy. The surface stability changes according to (110) > (101) > (010) > (001), and correlates well with the surface Pb coordination number and charge, i.e, surfaces are more stable the higher the Pb coordination number (which correlates with the atomic charge, as it has been pointed out above). This behaviour have already been observed in the case of the also rutile TiO_2 thin films, previously studied [13]. To the best of our knowledge, this is the first time the surface energies of β-PbO_2 have been obtained, which prevents comparison with other available data.

Having all this discussion on mind, we analysed the behaviour of the PbO_2 films due to the coating with SnO_2.

3.3. PbO_2 coated films

The purpose of this section is to analyse the changes caused in the PbO_2 films by the SnO_2 coating. As a first aspect to be noted, the PbO_2/SnO_2 slabs are slightly less thick than the pure PbO_2 ones (see Table 4), as a consequence of the smaller radius of the Sn atom. The band structure for the studied films was calculated through the same symmetry path used for the pure PbO_2 slabs (Fig. 4). It can be realized that the SnO_2 coating causes significative changes on the films band gap, with increases in the films with (001) and (010) surfaces, while a decrease is noticed in the band gap energy of the films with (110) and (101) surfaces. These results indicate that SnO_2 coating on PbO_2 surfaces is a practical way of having devices with the properties of SnO_2 surfaces and, in some cases, a better semiconductor behaviour than the pure PbO_2 films. On the other hand, since the pure SnO_2 band gap is 3.80 eV, these films will have a lower transparency than pure SnO_2 films (SnO_2 thin film exhibit a transmittance of around 90% in the 400–1100 nm interval and a direct energy band gap around 4.0 eV) [103].

Table 4
Thickness (Å) and surface energies ($J.m^{-2}$) values for the different pure PbO_2 and PbO_2/SnO_2 thin films.

planes	PbO_2		PbO_2/SnO_2	
	thickness	E_{surf}	thickness	E_{surf}
(110)	24.0	1.938	23.4	2.819
(101)	18.6	1.975	18.5	2.806
(010)	19.6	2.033	19.2	2.913
(001)	20.6	2.476	20.7	3.384

Strictly related to the BS, the DOS profiles of each slab are shown in Fig. 5, which help to analyse the orbital contribution for the slabs BS. As in the case of pure slabs, the valence band is predominantly constituted for O 2*p* orbitals (this orbital was not plotted since its amplitude is much greater than the other curves). The metallic *s* and *p* orbitals have a residual participation, with a slight predominance of *p* orbitals. On the other hand, the conduction band is basically composed of metallic s orbitals, with a minor contribution of Sn. This result agrees with the band gap energy of the coated films, much closer to the PbO_2 pure films band gap energy than to that of bulk SnO_2. From the point of view of the concentration, this is an expected result for the simulation, since the SnO_2 layer is much thinner than the PbO_2 film. However, the influence of the recovering is not so direct, since in some cases there are an increase in the films band gap energy, while in other cases that energy decreases.

The MPA atomic charge on the atoms of the Sn and O for the two firsts surface layers and the Pb and O atoms for the third and fourth ones is listed in Table 5.

In the same way that has been verified for the pure PbO_2 films, there is a significant diminution of the Sn and O charge when comparing to the SnO_2 bulk. This diminution occurs due to a charge transfer of Sn and O to the Pb and O atoms in the third and fourth layers. Besides, comparing the results in Tables 4 and 5, it is noticed that the charge on the Sn and O in the coated slabs are higher than on the corresponding Pb and O atoms in the pure ones, accordingly to the charges of the SnO_2 and PbO_2 bulks, which indicates a surface with a more accentuated ionic character when comparing to the pure slabs. The electrostatic isosurface potential of the surfaces for the PbO_2 pure films and PbO_2/SnO_2 bi-layer films is seen in the Fig. 6. It is observed that the doping with Sn atoms causes a small change in the charge distribution and modify positively the potential of the exposed facet.

Of course, it will be very interesting to analyse what happen to the surfaces stability after changing the surface Pb atoms for Sn. The energy obtained for each slab is listed in Table 3, and shows that the energies of the coated films are almost 1 J m^{-2} higher than the pure ones, which indicate a decrease in the surfaces stability when comparing to the pure slabs, suggesting surfaces more reactive that the pure PbO_2 ones. However, the relative stability of the surfaces virtually does not change because of the coating. Studies performed previously for the TiO_2/PbO_2

Table 3
The Mülliken atomic charge (e) in the firsts four surface layers of PbO_2 slabs.

Crystallographic planes	1[a] layer		2[a] layer		3[a] layer		4[a] layer	
	Pb	O	Pb	O	Pb	O	Pb	O
(0 0 1)	1.557	−0.746	1.787	−0.944	1.902	−0.933	1.896	−0.956
(0 1 0)	1.668	−0.732	1.882	−0.912	1.922	−0.965	1.932	−0.965
(1 0 1)	1.662	−0.760	1.871	−0.948	1.894	−0.944	1.894	−0.948
(1 1 0)	1.758	−0.784	1.877	−0.839	1.920	−0.958	1.902	−0.954

Table 5
The atomic charge (e) on first and second surface layers Sn and O atoms, and Pb and O for the third and fourth surface layers of the PbO_2/SnO_2 slabs.

Crystallographic planes	1st layer		2nd layer		3rd layer		4th layer	
	Sn	O_{Sn}	Sn	O_{Sn}	Pb	O_{Pb}	Pb	O_{Pb}
(0 0 1)	1.863	−0.898	2.131	−1.086	1.971	−0.994	1.945	−0.981
(0 1 0)	1.950	−0.889	2.240	−1.130	1.995	−1.042	1.970	−0.986
(1 0 1)	1.961	−0.928	1.948	−0.964	1.933	−0.967	1.933	−0.965
(1 1 0)	1.994	−0.929	1.990	−0.985	1.961	−1.068	2.018	−1.005

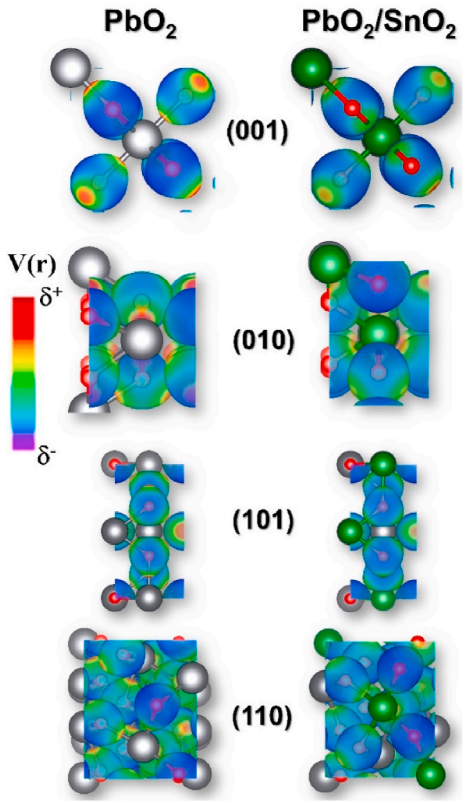

Fig. 6. Top view of surface electrostatic potential [$V_S(r)$] for pure films (right), and PbO_2/SnO_2 films (left). The blue and red color denotes positive and negative charge densities, respectively.

[13], and TiO_2/SnO_2[9] systems shown an exchange in the relative stability of TiO_2 surfaces coated with PbO_2 and SnO_2 oxides, respectively. The present study indicates that this behaviour is not universal. It is interesting to draw the attention that in both previous studies the surface Ti atom of the original pure films have been changed for larger atoms, while in the nowadays study, the surface Pb atoms of the pure film have been changed for smaller ones. As a result of maintaining the relative stability of surfaces when comparing pure and coated films, the preferential grow direction and the crystalline shape of the films is maintained. Thus, the coating of PbO_2 with SnO_2 does not cause significant morphological changes in the pure PbO_2 films. The calculation of the surface energies allows for morphology estimation using the Wulff's construction. Along with the study of the construction and structure determination of the covered PbO_2 thin films, it is also interesting to understand how a nanoparticle of this system can behaves if existing. At this point, it is important to point out that the calculated morphology represents the system without environmental influences and interactions with the environment need to be taken into account in order to understand a given experimental morphology. However, it is possible to impose a given surface energy to delimit the external potential and find the possible morphological paths, which include the studied surfaces [86]. With this in mind a morphological mapping was calculated starting from the calculated E_{surf}, and assuming energy modulation between (hkl) indices, to understand how the variation of surface energy can determine which crystal facet is exposed [86], which can directly be associated to the environment of synthesis, as shown in Fig. 7a and b. In Fig. 7a, it is possible to see the equilibrium crystals for the PbO_2 and PbO_2/SnO_2, constructed with energies supplied in Table 3 together with the equal surface energies from all facets. This Wulff's construction (Fig. 7a) shows that pure PbO_2 has the (010), (101) and (110) facets, without the presence of the (001) facet, however when the coverage is considered the (001) facet starts to be exposed and compose approximately ~0.08% of the exposed surfaces. Also it is shown the equal surface energy crystal for comparison purposes.

Fig. 7b) show the map of the possible morphological transformations of the system in each possible growing environment. To do this mapping we had normalized the surface energy, defining a surface energy ratio ($\Gamma^* = \Gamma_{(hkl)}/\Gamma_{(001)}$) and finding this ratio for the maximum exposure of each facet, which we named v_1, v_2, v_3, v_4 and v_5, where the last one is the PbO_2/SnO_2 crystal (details on this construction can be find in ref. 86). The surface ratio energy and their maximum values are highlighted in the Fig. 7b. It is interesting to note that the pure PbO_2 crystal can be found in the middle of the path between the v_3 and the center of the Wulff's map (v_5). Besides that, the other morphologies can be associated to the environmental and synthesis method, as the crystal shape are strongly dependent of those variables.

Considering the Wulff construction and the surface array energy depicted in Fig. 7b), it is possible estimate the DOS of a possible nanoparticle of PbO_2 covered with a thin layer of SnO_2, where the contribution of each exposed surface was weighted with the exposed area as shown with the pie graphic in Fig. 8.

Fig. 8 shows the individual contribution for the DOS of each one of the exposed planes of the nanoparticle, estimating the energy range where each one have a major role when searching for properties of individual nanoparticles. This analysis is an interesting tool to understand more on each facet behaves, and its contribution for the electronic properties in general, and also can be useful to understand the morphology of experimental solid-state microscopic particles. However, although this methodology can be an indicative of the band gap energy, it difficulty can be directly compared to experimental results, since these are strongly dependent on the synthesis methods and experimental parameters, like pressure, temperature, and environment, among others.

4. Conclusions

Surface and electronic properties of PbO_2 and PbO_2 coated with SnO_2 thin films with crystallographic planes (001), (010), (101), and (110), have been investigated through periodic quantum mechanics DFT calculations. The results show significant increases in the band gap energy of the pure PbO_2 films compared to that of the bulk, due to a significative increase in the minimum energy of the conduction band. Thus, thin films reduce the conductivity of the material and brings its properties closer to those of a semiconductor. This behaviour can make films suitable for new applications, unfeasible for pure bulk. The surfaces are less oxidant and the atom bonds are more covalent than the bulk itself. The relative surface stability follows the sequence (110) > (101) > (010) > (001). The surfaces become more unstable, and with a more accentuated ionic character after coating with SnO_2, however, the relative stability of the

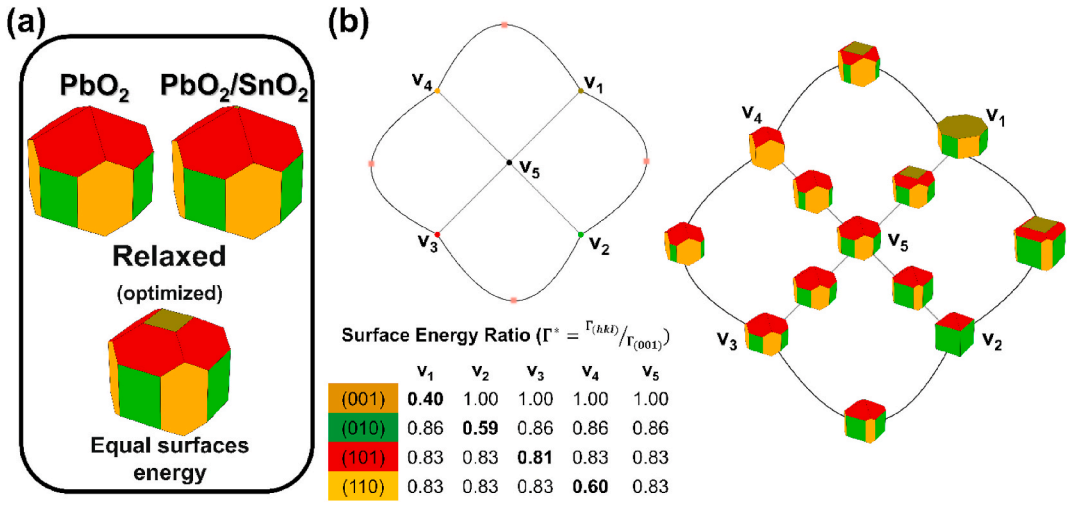

Fig. 7. (a) Wulff's construction morphology of the optimized bulk PbO_2 and the SnO_2 covered nanoparticle, and (b) the morphology graph with all possible estimated variations of the crystal in function of the surface energy of each exposed facet. Each v_i represents a Wulff crystal built to expose the highest percentage area of a specific plane (hkl), and the other crystals are the intermediated shapes between two specific morphologies.

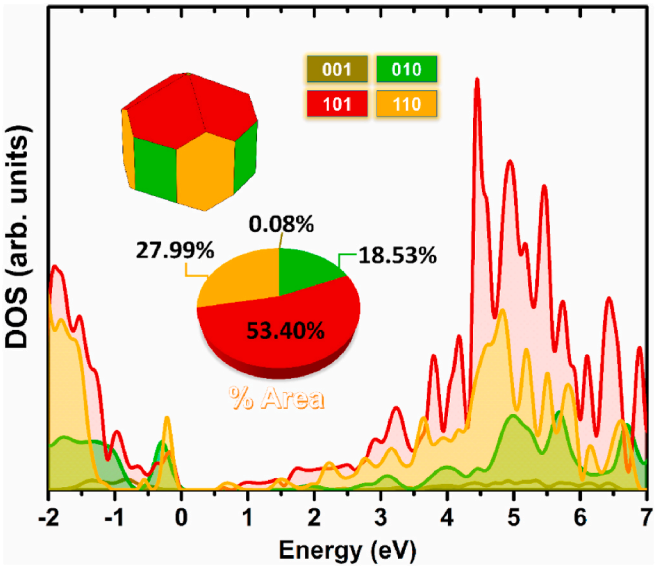

Fig. 8. Estimative of the density of states of the PbO_2/SnO_2 nanoparticle.

surfaces does not change. Thus, the preferential grow direction and the crystalline shape of the coated films is maintained. The SnO_2 coating causes significative changes on the films band gap, with increases in the films with (001) and (010) surfaces, while a decrease is noticed in the band gap energy of the films with (110) and (101) surfaces. These results indicate that SnO_2 coating on PbO_2 surfaces is a practical way of having devices with the properties of SnO_2 surfaces but with a better semiconductor behaviour than the pure PbO_2 films. On the other hand, since the pure SnO_2 band gap is 3.80 eV, these films will have a lower transparency than pure SnO_2 films.

Credit author contribution statement

G.S.L. Fabris: Software, Validation, Methodology, Visualization, Investigation, Formal analysis, Writing - review & editing. D.H.M. Azevedo: Software, Methodology, Visualization, Formal analysis. A.C. Alves and C.A. Paskocimas: Software, Methodology. J.R. Sambrano: Conceptualization, Funding acquisition, Methodology, Project administration, Resources, Software, Writing - review & editing. J.M.M. Cordeiro: Conceptualization, Investigation, Methodology, Supervision, Project administration, Resources, Writing - original draft, Writing - review & editing.

Data availability

The data needed to reproduce the findings are available in the body of the text.

Declaration of competing interest

The authors declare that they have no known competing financial interests or personal relationships that could have appeared to influence the work reported in this paper.

Acknowledgments

This work is supported by Brazilian Funding Agencies: CNPq (461264, 482473/2010-0, 446126/2014-4, 308548/2014-0, 307236/2018-8), CAPES (787027/2013, 8881.068492/2014-01), FAPESP (2013/07296-2, 2019/08928-9). Guilherme S. L. Fabris thanks the postdoc scholarship financed by the Coordenação de Aperfeiçoamento de Pessoal de Nível Superior - Brasil (CAPES) - Finance Code 001 – (grant no. 88887.467334/2019-00). The computational facilities were supplied by Molecular Simulations Laboratory, São Paulo State University, Bauru, Brazil, and Laboratory of Computational Chemistry, São Paulo State University, Ilha Solteira, Brazil.

References

[1] E. Fortunato, P. Barquinha, R. Martins, Adv. Mater. 24 (2012) 2945.
[2] B.C.K. Tee, A. Chortos, A. Berndt, A.K. Nguyen, A. Tom, A. McGuire, Z.L. C Lin, K. Tien, W.G. Bae, H.L. Wang, P. Mei, H.H. Chou, B.X. Cui, K. Deisseroth, T.N. Ng, Z.N. Bao, Science 350 (2015) 313.
[3] X. Yu, T.J. Marks, A. Facchetti, Nat. Mater. 15 (2016) 383.
[4] G. Han, S. Zhang, P.P. Boix, Prog. Mater. Sci. 87 (2017) 246.
[5] J.Z. Bloh, R. Marshall, Eur. J. Org Chem. 15 (2017) 2085.
[6] L.H. Oliveira, M.A. Ramírez, M.A. Ponce, L.A. Ramajo, A.R. Albuquerque, J. R. Sambrano, E. Longo, M.S. Castro, F.A. La Porta, Mater. Res. Bull. 93 (2017) 47.
[7] A.F.V. Fonseca, R.L. Siqueira, R. Landers, J.L. Ferrari, N.L. Marana, J. R. Sambrano, F.A. La Porta, M.A. Schiavon, J. Alloys Compd. 739 (2018) 939.
[8] T.M. Mazzo, L.R. Macario, L.F. Gorup, V. Bouquet, S. Deputier, S. Ollivier, M. Guilloux-Viry, A.R. Albuquerque, J.R. Sambrano, F.A. La Porta, E. Longo, ACS Appl. Nano Mater. 2 (2019) 2612.
[9] R. Inguanta, S. Piazza, C. Sunseri, J. Electrochem. Soc. 155 (2008) K205.
[10] P. Perret, T. Brousse, D. Belanger, D. Guay, J. Electrochem. Soc. 156 (2009) A645.
[11] P.N. Bartlett, T. Dunford, M.A. Ghanem, J. Mat. Chem. 12 (2002) 3130.

[12] A. Beltran, J. Andres, J.R. Sambrano, E. Longo, J. Phys. Chem. 112 (2008) 8943.
[13] D.H.M. Azevedo, G.S.L. Fabris, J.R. Sambrano, J.M.M. Cordeiro, Comput. Mater. Sci. 171 (2020) 109222.
[14] X. Li, D. Pletcher, F.C. Walsh, Chem. Soc. Rev. 40 (2011) 3879.
[15] D.J. Payne, R.G. Egdell, G. Paolicelli, F. Offi, G. Panaccione, P. Lacovig, G. Monaco, G. Vanco, A. Walsh, G.W. Watson, J. Guo, G. Beamson, P.A. Glans, T. Learmonth, K.E. Smith, Phys. Rev. B 75 (2007) 153102.
[16] D.J. Payne, R.G. Egdell, D.S.L. Law, P.A. Glans, T. Learmonth, K.E. Smith, J. Guo, G.W. Watson, A. Walsh, J. Math. Chem. 17 (2007) 267.
[17] D.J. Payne, R.G. Egdell, W. Hao, J.S. Foord, A. Walsh, G.W. Watson, Chem. Phys. Lett. 411 (2005) 181.
[18] D.J. Payne, G. Paolicelli, F. Offi, G. Panaccione, P. Lacovig, G. Beamson, A. Fondacaro, G. Monaco, G. Vanko, R.G. Egdell, J. Electron. Spectrosc. Relat. Phenom. 169 (2009) 26.
[19] S. Abaci, K. Pekmez, A. Yildiz, Electrochem. Commun. 7 (2005) 328.
[20] A. Walsh, A.B. Kehoe, D.J. Temple, G.W. Watson, D.O. Scanlon, Chem. Commun. 49 (2013) 448.
[21] D.O. Scanlon, A.B. Kehoe, G.W. Watson, M.O. Jones, W.I.F. David, D.J. Payne, R. G. Egdell, P.P. Edwards, A. Walsh, Phys. Rev. Lett. 107 (2011) 246402.
[22] S. Rothenberg, D.J. Payne, A. Bourlange, R.G. Egdell, J. Appl. Phys. 102 (2007) 113717.
[23] J.M.M. Cordeiro, D.H.M. Azevedo, T.C.M. Barreto, J.R. Sambrano, Mat. Res. 21 (2018) 20170641.
[24] M. Burbano, D.O. Scanlon, G.W. Watson, J. Am. Chem. Soc. 133 (2011) 15065.
[25] Y. Yang, S. Jin, J.E. Medvedeva, J.R. Ireland, A.W. Metz, J. Ni, M.C. Hersam, A. J. Freeman, T.J. Marks, J. Am. Chem. Soc. 127 (2005) 8796.
[26] T.S. Moss, Proc. Phys. Soc. B 67 (1954) 775.
[27] E. Burstein, Phys. Rev. 93 (1954) 632.
[28] C. Kílíç, A. Zunger, Phys. Rev. Lett. 88 (2002), 095501.
[29] D. Segev, S.H. Wei, Phys. Rev. B 71 (2005) 125129.
[30] F.R. Costa, L.M. Silva, Quim. Nova 35 (2012) 962.
[31] M. Panizza, G. Cerisolla, Chem. Rev. 109 (2009) 6541.
[32] L. Fan, Y. Zhou, W. Yang, G. Chen, F. Yang, J. Hazard Mater. 137 (2006) 1182.
[33] A.S. Koparal, Y. Yavuz, C. Gurel, U.B. Ögutveren, J. Hazard Mater. 145 (2007) 100.
[34] Z. Wang, G. Wang, Phys. Lett. 381 (2017) 2856.
[35] W. Wang, L. Deng, N. Jiao, P. Zhou, L. Sun, Phys. Status Solidi 11 (2017) 1700271.
[36] S. Mahatara, B. Kiefer, J. Phys. Condens. Matter 32 (2020) 255504.
[37] S. Gubbala, V. Chakrapani, V. Kumar, M.K. Sunkara, Adv. Funct. Mater. 18 (2008) 2411.
[38] Y. Fukai, Y. Kondo, S. Mori, E. Suzuki, Electrochem. Commun. 9 (2007) 1439.
[39] J.M. Smulko, J. Ederth, Y. Li, L.B. Lish, M.K. Kennedy, F.E. Kruis, Sens. Actuators, B 106 (2005) 708.
[40] E.A. Floriano, L.V.A. Scalvi, M.J. Saeki, J.R. Sambrano, J. Phys. Chem. 118 (2014) 5857.
[41] W. Gopel, K.D. Schierbaum, Sensor. Actuator. B Chem. 26 (1995) 1.
[42] S. Kufner, A. Schleife, B. Hoffling, F. Bechstedt, Phys. Rev. B 86 (2012), 075320.
[43] R. Rai, T.D. Senguttuvan, S.T. Lakshmikumar, Comput. Mater. Sci. 37 (2006) 15.
[44] J. Bruneaux, H. Cachet, M. Froment, A. Messad, Thin Solid Films 197 (1991) 129.
[45] S.V. Eremev, O.I. Velikokhatnyi, P.N. Kimta, A.I. Potekaev, Russ. Phys. J. 47 (2004) 701.
[46] K.S. Kim, S.Y. Yoon, W.J. Lee, K.H. Kim, Surf. Coating. Technol. 138 (2001) 229.
[47] Q.J. Liu, Z.T. Liu, L.P. Feng, Comput. Mater. Sci. 47 (2010) 1016.
[48] C. Ponce, M. Caravaca, R. Casali, J. Phys. Chem. C 119 (2015) 15604.
[49] F.K. Butt, C.B. Cao, W.S. Khan, Z. Ali, T. Mahmood, R. Ahmed, S. Hussain, G. Nabi, Mater. Chem. Phys. 136 (2012) 10.
[50] F.K. Butt, C.B. Cao, W.S. Khan, M. Safdar, X.W. Fu, M. Tahir, F. Idrees, Z. Ali, G. Nabi, D.P. Yu, CrystEngComm 15 (2013) 2106.
[51] F.K. Butt, C.B. Cao, R. Ahmed, W.S. Khan, Z. Ali, S. Hussain, F. Idrees, M. Tahir, J. Exp. Nanosci. 9 (2014) 17.
[52] M. Akram, A.Z. Alshemary, F.K. Butt, Y.F. Goh, W.A.W. Ibrahim, R. Hussain, Mater. Lett. 160 (2015) 146.
[53] F.K. Butt, A.S. Bandarenka, J. Solid State Electrochem. 20 (2016) 2915.
[54] R.A. Casali, J. Lasave, M.A. Caravaca, S. Koval, C.A. Ponce, R.L. Migoni, J. Phys. Condens. Matter 25 (2013) 135404.
[55] A.M. Ganose, D.O. Scanlon, J. Mater. Chem. C 4 (2016) 1467.
[56] P.D. Borges, L.M.R. Scolfaro, H.W.L. Alves, E.F. da Silva, Theor. Chem. Acc. 126 (2010) 39.
[57] S. Tingting, Z. Fuchun, Z. Weihu, Z. Rare Metal Mater. Eng. 44 (2015) 2409.
[58] R. Gilani, S.U. Rehman, F.K. Butt, B.U. Haq, F. Aleem, Siliconindia 10 (2018) 2317.
[59] F.A. Akgul, C. Gumus, A.O. Er, A.H. Fahra, G. Akgul, Y. Ufuktepe, Z. Liu, J. Alloys Compd. 579 (2013) 50.
[60] G.G. Almeida, J.M.M. Cordeiro, M.E. Martin, M.A. Aguilar, J. Chem. Theor. Comput. 12 (2016) 1514.
[61] A. Borges, J.M.M. Cordeiro, Chem. Phys. Lett. 565 (2013) 40.
[62] J. Claverie, F. Bernard, J.M.M. Cordeiro, S. Kamali-Bernard, J. Phys. Chem. Solid. 132 (2019) 48.
[63] J. Claverie, F. Bernard, J.M.M. Cordeiro, S. Kamali-Bernard, Cement Concr. Res. 136 (2020) 106162.
[64] A.D. Becke, J. Chem. Phys. 98 (1993) 56485652.
[65] C. Lee, W. Yang, G.R. Parr, Phys. Rev. B 37 (1988) 785.
[66] S. Grimme, J. Comput. Chem. 25 (2004) 1463.
[67] S. Grimme, J. Comput. Chem. 27 (2006) 1787.
[68] J. Haines, J.M. Léger, Phys. Rev. B 55 (1997) 11144.
[69] R. Dovesi, A. Erba, R. Orlando, C.M. Zicovich-Wilson, B. Civalleri, L. Maschio, M. Rérat, S. Casassa, J. Baima, S. Salustro, B. Kirtman, Comp. Mol. Sci. 8 (2018), e1360.
[70] C. Pisani, R. Dovesi, C. Roetti, Hartree-Fock Ab Initio Treatment of Crystalline Systems, Springer-Verlag, Berlin Heidelberg, 1988.
[71] C. Gatti, V.R. Saunders, C. Roetti, J. Chem. Phys. 101 (1994) 10686.
[72] A.R. Albuquerque, I.M.G. Santos, J.R. Sambrano, Quim. Nova 37 (2014) 1318.
[73] J. Maul, A. Erba, I.M.G. Santos, J.R. Sambrano, R. Dovesi, J. Chem. Phys. 142 (2015), 014515.
[74] T.M. Duarte, P.G.C. Buzolin, I.M.G. Santos, E. Longo, J.R. Sambrano, Theor. Chem. Acc. 135 (2016) 151.
[75] E.O. Gomes, G.S.L. Fabris, M.M. Ferrer, F.V. Motta, M.R.D. Bomio, J. Andres, E. Longo, J.R. Sambrano, Comput. Mater. Sci. 170 (2019) 109176.
[76] J. Maul, I.M.G. Santos, J.R. Sambrano, A. Erba, Theor. Chem. Acc. 135 (2016) 36.
[77] E. Heifets, R.I. Eglitis, E.A. Kotomin, J. Maier, G. Borstel, G. *Surf. Sci.* 513 (2002) 211.
[78] K. Lejaeghere, G. Bihlmayer, T. Björkman, P. Blaha, S. Blügel, V. Blum, Science 351 (2016) aad3000.
[79] S.F. Souza, P.A. Fernandes, M.J. Ramos, J. Phys. Chem. 111 (2007) 10439.
[80] H.J. Monkhorst, J.D. Pack, Phys. Rev. B 13 (1976) 5188.
[81] R. Tran, Z. Xu, B. Radhakrishnan, D. Winston, W. Sun, K.A. Persson, S.P. Ong, Sci. Data 3 (2016) 160080.
[82] S.D. Lazaro, R.F. Penteado, S.M. Tebcherani, D. Berger, J.A. Varela, E.T. Kubaski, Quím. Nova 35 (2012) 920.
[83] G.Z.Z. Wulff, Kristallografiya 34 (1901) 449.
[84] A.F. Gouveia, M.M. Ferrer, J.R. Sambrano, J. Andrés, E. Longo, Chem. Phys. Lett. 660 (2016) 87.
[85] M.A. Barbosa, G.S.L. Fabris, M.M. Ferrer, D.H.M. Azevedo, J.R. Sambrano, Mat. Res. 20 (2017) 920.
[86] J.A.S. Laranjeira, G.S.L. Fabris, M.M. Ferrer, A.R. Albuquerque, J.R. Sambrano, Cryst. Growth Des. 20 (2020) 4600.
[87] J. Claverie, S. Kamali-Bernard, J.M.M. Cordeiro, F. Bernard, Cement Concr. Res. 140 (2021) 106269.
[88] M. Nizam, Y. Bouteiller, B. Silvi, C. Pisani, M. Causa, R. Dovesi, J. Phys. C Solid State Phys. 21 (1988) 5351.
[89] M. Causa, R. Dovesi, C. Roetti, Phys. Rev. B 43 (1991) 11937.
[90] M. Calatayud, J. Andrés, A. Beltran, Surf. Sci. 430 (1999) 213.
[91] G. Sophia, P. Baranek, C. Sarrazin, M. Rérat, R. Dovesi, Phase Transitions 86 (2013) 1069.
[92] J. Laun, D.V. Oliveira, T. Bredow, J. Comput. Chem. 39 (2018) 1285.
[93] D.P. Rai, A. Laref, A. Shankar, Sandeep, A.P. Sakhya, R. Khenata, R.K. Thapa, J. Phys. Chem. Solid. 120 (2018) 104.
[94] A. Katoch, G.-J. Sun, S.-W. Choi, S. Hishita, V.V. Kulish, P. Wu, S.S. Kim, Sci. Rep. 4 (2014) 4622.
[95] O. Mounkachi, E. Salmani, M. Lakhal, H. Ez-Zahraouy, M. Hamedoun, M. Benaissa, A. Kara, A. Ennaoui, A. Benyoussef, Sol. Energy Mater. Sol. Cells 148 (2016) 34.
[96] L. Gracia, A. Beltran, J. Andres, J. Phys. Chem. B 111 (2007) 6479.
[97] H. Hosono, Thin Solid Films 515 (2007) 6000.
[98] A. Splendiani, L. Sun, Y. Zhang, T. Li, J. Kim, C.Y. Chim, G. Galli, F. Wang, Nano Lett. 10 (2010) 1271.
[99] K.F. Mak, C. Lee, J. Hone, J. Shan, T.F. Heinz, Phys. Rev. Lett. 105 (2010) 136805.
[100] V.M. Longo, F.C. Picon, C. Zamperini, A.R. Albuquerque, J.R. Sambrano, C. E. Vergani, A.L. Machado, J. Andrés, A.C. Hernandes, J.A. Varela, E. Longo, Chem. Rev. Letters 577 (2013) 114.
[101] P.W. Tasker, J. Phys. C Solid State Phys. 12 (1979) 4977.
[102] C. Noguera, J. Phys. Condens. Matter 12 (2000) R367.
[103] O. Erken, O.M. Ozkendir, M. Gunes, E. Harputlu, C. Ulutas, C. Gumus, Ceram. Int. 45 (2019) 19086.